HHS Public Access

Author manuscript

J Huntingtons Dis. Author manuscript; available in PMC 2018 December 28.

Published in final edited form as:

J Huntingtons Dis. 2018 ; 7(1): 35–50. doi:10.3233/JHD-170266.

Inhibition of TRPC1-Dependent Store-Operated Calcium Entry Improves Synaptic Stability and Motor Performance in a Mouse Model of Huntington's Disease

Jun Wu[a], **Daniel Ryskamp**[a], **Lutz Birnbaumer**[b,c], and **Ilya Bezprozvanny**[a,d,*]

[a]Department of Physiology, University of Texas Southwestern Medical Center, Dallas, TX, USA

[b]Neurobiology Laboratory, NIEHS, Research Triangle Park, NC, USA

[c]Institute of Biomedical Research (BIOMED), Catholic University of Argentina, C1107AFF Buenos Aires, Argentina

[d]Laboratory of Molecular Neurodegeneration, Peter the Great St. Petersburg Polytechnic University, St. Petersburg, Russia

Abstract

Background: Huntington disease (HD) is a dominantly inherited neurodegenerative disorder caused by a CAG repeat expansion in the *huntingtin* gene. We previously discovered that mutant Huntingtin sensitizes type 1 inositol 1,4,5-trisphosphate receptor ($InsP_3R1$) to $InsP_3$. This causes calcium leakage from the endoplasmic reticulum (ER) and a compensatory increase in neuronal store-operated calcium (nSOC) entry. We previously demonstrated that supranormal nSOC leads to synaptic loss in striatal medium spiny neurons (MSNs) in YAC128 HD mice.

Objective: We sought to identify calcium channels supporting supranormal nSOC in HD MSNs and to validate these channels as potential therapeutic targets for HD.

Methods: Cortico-striatal cultures were established from wild type and YAC128 HD mice and the density of MSN spines was quantified. The expression of candidate nSOC components was suppressed by RNAi knockdown and by CRISPR/Cas9 knockout. TRPC1 knockout mice were crossed with YAC128 HD mice for evaluation of motor performance in a beamwalk assay.

Results: RNAi-mediated knockdown of TRPC1, TRPC6, Orai1, or Orai2, but not other TRPC isoforms or Orai3, rescued the density of YAC128 MSN spines. Knockdown of stromal interaction molecule 1 (STIM1), an ER calcium sensor and nSOC activator, also rescued YAC128 MSN spines. Knockdown of the same targets suppressed supranormal nSOC in YAC128 MSN spines. These channel subunits co-immunoprecipitated with STIM1 and STIM2 in synaptosomal lysates from mouse striata. Crossing YAC128 mice with TRPC1 knockout mice improved motor performance and rescued MSN spines *in vitro* and *in vivo*, indicating that inhibition of TRPC1 may serve as a neuroprotective strategy for HD treatment.

*Correspondence to: Dr. Ilya Bezprozvanny, 5323 Harry Hines Blvd., ND12.200, Dallas, TX 75390, USA. Ilya.Bezprozvanny@UTSouthwestern.edu.

CONFLICT OF INTEREST

The authors have no financial conflict of interest in relation to results described in the paper.

Conclusions: TRPC1 channels constitute a potential therapeutic target for treatment of HD.

Keywords

Huntingtin; synaptic; store-operated calcium entry; TRPC1; STIM1; imaging; beamwalk

INTRODUCTION

Huntington's disease (HD) is an autosomal dominant, neurodegenerative disorder caused by a CAG repeat expansion in the *huntingtin* gene, encoding polyglutamine-expanded mutant Huntingtin (mHtt) protein [1]. In spite of widespread expression of mHtt in the brain, the striatum is disproportionally affected and suffers progressive atrophy. The cerebral cortex and thalamus are also affected but to a lesser extent [2–4]. HD is clinically characterized by motor disturbances (e.g., chorea), cognitive decline, and psychiatric symptoms. The appearance of symptoms parallels the subtle changes in neuronal function and synaptic plasticity at early stages of HD pathology [5–9]. Later on there is a progressive loss of striatal medium spiny neurons (MSNs). Currently approved HD therapeutics are limited to symptomatic care (e.g., tetrabenazine and deutetrabenazine for management of chorea) and neglect the pathophysiological processes underlying disease initiation and progression [4, 10, 11]. Fortunately, this is an active area of clinical development, with several ongoing clinical trials [12]. Gene therapies that lower levels of mHtt are particularly promising, such as the targeting of mHtt mRNA by anti-sense oligonucleotides [12]. Pridopidine may also have disease-modifying properties [13] and has exhibited preliminary therapeutic potential in clinical trials [14–17]. As disease-modifying treatments are still needed for HD, identification of viable therapeutic targets remains an important pursuit.

In our previous work, we found that mHtt dysregulates calcium (Ca^{2+}) homeostasis by directly sensitizing the endoplasmic reticulum (ER) ion channel inositol 1,4,5-trisphosphate receptor type 1 ($InsP_3R1$) to $InsP_3$ [18, 19]. We reasoned that the resulting Ca^{2+} dysregulation contributes to the vulnerability of MSNs [20, 21]. Increased activity of $InsP_3R1$ leads to excessive Ca^{2+} leakage and depletion of Ca^{2+} in the ER. To compensate for calcium leakage and depletion from the ER, HD MSNs upregulate neuronal store-operated calcium (nSOC) entry to synaptotoxic levels [22]. Normalization of the nSOC pathway — by knocking down $InsP_3R1$ or the ER calcium sensor STIM2 —prevented dendritic spine loss in YAC128 MSNs in aged corticostriatal co-cultures [22]. Also, blocking supranormal nSOC with a chemical inhibitor that was identified as beneficial in a screen with HD-afflicted flies [23] rescues YAC128 MSN spines both *in vitro* and *in vivo* [22]. These results suggest that the nSOC pathway is involved in the pathogenesis of HD and can potentially provide novel targets for therapeutic intervention.

In non-excitable cells SOC is mediated by TRPC and/or Orai channel subunits, which are regulated by STIM1 or STIM2 ER Ca^{2+} sensor proteins [24]. The molecular composition of the nSOC pathway in MSNs is less established, but most likely it is also comprised of TRPC and/or Orai family members. Orai and TRPC channels are expressed in the nervous system [25–28]. In the present work, we systematically investigated the involvement of putative SOC components in WT and YAC128 MSN spine stability. We found that TRPC3, TRPC4,

and TRPC5 were required for WT MSN spine stability. TRPC1, TRPC6, Orai1 and Orai2 were not required for WT MSN spine stability, but knocking them down rescued YAC128 MSN spines by lowering nSOC below synaptotoxic levels. Likewise, knockdown of STIM1 preserved YAC128 spines without disrupting WTMSN spines.STIM1andSTIM2preferentially formed complexes with TRPC1, TRPC6, Orai1 and Orai2 in synaptosomal lystates from WT mouse striata. Furthermore, crossing YAC128 mice with TRPC1 knockout mice leads to suppressed spine nSOC, the rescue of YAC128 MSN spines *in vitro* and *in vivo*, and improved motor performance.

MATERIALSANDMETHODS

RNAi, lenti-viruses, and validation by western blotting

Control short-hairpin RNA interference (Ctrl-shRNAi) (SHC002), mouse TRPC1-shRNAi (SHCLNG-NM_ 011643, TRCN0000305050), mouse TRP C3-shRNAi (SHCLNG-NM_019510,TRCN0000422735), mouse TRPC4-shRNAi (SHCLNG-NM_016984, TRCN0000068324), mouse TRPC5-shRNAi (SHCLNG-NM_009428, TRCN000 0449041), mouse TRPC6-shRNAi SHCLNG-NM_013838, TRCN000 0068394), mouse Stim1-shRNAi (SHCLNG-NM_009287, TRCN0000193400), mouse Orai1-shRNAi (SHCLNG-NM_175423, TRCN0000125405), mouse Orai2-shRNAi (SHCLNG-NM_178751, TRCN0000 126314), and mouse Orai3-shRNAi (SHCLNG-NM_198424, TRCN0000250865) lentivirus shuttle constructs were obtained from Sigma-Aldrich. Lentiviruses were generated by co-transfection of two helper plasmids (pVSVg and pCMVΔ8.9) into the packaging cell line HEK293T, as we described previously [29]. Western blotting was used to analyze siRNA-mediated knockdown of TRPC and Orai isoforms in at least two batches of corticostriatal co-cultures. For this, cultures were infected with lenti-virus particles on day *in vitro* (DIV) 7 and were lysed on DIV14–15 with 1X SDS sample buffer. Samples were sonicated on ice and heated at 90°C for 2–3min. Samples were then subjected to SDS-PAGE and transferred using a Trans-Blot Turbo (Bio-Rad). Membranes were stained with primary and then secondary antibodies (listed below) in TBST with 5% BSA, washing with TBST after each step. HRP activity was detected with western Lighting Plus-ECL (PerkinElmer) and an X-ray film developer. Because the lenti-viruses we use exhibit selective tropism for neurons in our cultures [22], glial protein remains in the background. For quantification with ImageJ, the integrated density of each band was normalized to the corresponding tubulin band.

Antibodies

Anti-TRPC1 mAb (1:200, sc-133076, Santa Cruz Biotechnology), anti-TRPC3 pAb (1:400, PA5–20258, Thermo Scientific), anti-TRPC4 pAb (1:400, AB5812, Chemicon), anti-TRPC5pAb (1:1000, sc-18737, Santa Cruz Biotechnology), anti-TRPC6 pAb (1:500, SAB4300572, Sigma-Aldrich), anti-Stim1 pAb (1:1000, 4916s, Cell Signaling Technology), anti-Orai1 pAb (1:200, sc-68895, Santa Cruz Biotechnology), anti-Orai2 pAb (1:200, sc-292103, Santa Cruz Biotechnology) and anti-DARPP-32 mAb (1:500; 2306s, Cell Signaling Technology) were used. Goat anti-rabbit Alexa Fluor 488 secondary antibody (1:1000, 111–545-144), goat anti-rabbit Alexa Fluor 594 secondary antibody (1:1000, 111–

585-144), HRP-conjugated anti-mouse (115–035-146) and anti-rabbit secondary antibodies (111–035-144) were from Jackson ImmunoReseach.

Mice

Experiments involving mice were approved by the Institutional Animal Care and Use Committee of the University of Texas Southwestern Medical Center at Dallas and followed the National Institutes of Health Guidelines for the Care and Use of Experimental Animals. The TRPC1$^{-/-}$(129S) mice [30] were obtained from the Comparative Medicine Branch of the National Institute of Environmental Health Sciences, NIH, USA. This line was maintained by crossing homozygous animals. YAC128 transgenic (FVB-Tg(YAC128)53Hay/J; Jackson Labs: stock # 004938) mice [31] were crossed to the homozygous TRPC1$^{-/-}$ mice for 6 generations to obtain YAC128$^{+/-}$TRPC1$^{-/-}$ mice on the FVB background. The YAC128$^{+/-}$TRPC1$^{-/-}$line was maintained by crossing YAC128$^{+/-}$TRPC1$^{-/-}$ mice with TRPC1$^{-/-}$ mice after backcrossing. The presence of the YAC128 transgene was confirmed by genotyping with primers specific for exons 44 and 45 of human Htt gene. Both the TRPC1$^{-/-}$ and YAC128$^{+/-}$ TRPC1$^{-/-}$ mice were healthy and fertile. All the mice including wild type (WT; FVB/NJ) mice were maintained at UT Southwestern Medical Center in a barrier facility (12h light/dark cycle).

Real-time PCR and RT-PCR

We used real time-PCR (qPCR) as in [30] to confirm the absence of exon 8 of TRPC1 in TRPC1$^{-/-}$ mice with forward 5'-GCAACCTTTGCCCTCAAAGTG and reverse 5'-GGAGGAACATTCCCAGAAATTTCC primers. Total RNA was extracted from WT and TRPC$^{-/-}$ mouse striata using TRIzol (Invitrogen). To synthesize cDNA by reverse transcription, we used a High-Capacity RNA-to-cDNA Kit. Each well contained 25 ng of cDNA, each primer at 150 nM, and 5μl of 2×SYBR Green PCR Master Mix (ThermoFisher Scientific) and the final volume was 10μl. RT-PCR was performed using an Applied Biosystems Prism 7900HT sequence detection system. In parallel, we ran a RT PCR reaction with the same cDNA and the pair of primers and after 30 PCR cycles, the RT-PCR product was analyzed by 1% agarose gel electrophoresis.

Striatal synaptosome preparation, co-immunoprecipitation and western blotting experiments

Striatal regions were extracted from 1-month-old mice, homogenized in 0.32M sucrose and 25mM HEPES, pH 7.2, and centrifuged for 10 min at 800 × g to remove the nuclei. The low-speed supernatant was then centrifuged for 20min at 12,000 × g to separate the synaptosomal supernatant and synaptosomal membrane fractions (P2 pellet). The P2 pellets were solubilized in lysis buffer containing 1% CHAPS plus the following (in mM): 137 NaCl, 2.7 KCl, 4.3 Na_2HPO_4, 1.4 KH_2PO_4, pH 7.2, 5 EDTA, and 5 EGTA and protease inhibitors for 2h at 4°C. Insoluble material was removed by centrifugation of samples for 20min at 16,300 × g. The protein concentration in the synaptosome fraction was measured with a Nanodrop OD280. For each coimmunoprecipitation reaction, 500 μg of total protein lysates were first precleaned with normal rabbit, mouse, or goat IgG and protein A/G beads at 4°C for 1h, then incubated with 2μg of primary antibody at 4°C for 1h (or 2μg of the IgG control), and incubated with 20 μl of protein A/G agarose beads at 4°C overnight on a

rocking platform. Precipitated samples were then washed three times with lysis buffer, the final bead pellet was resuspended in 1×SDS loading buffer, and analyzed by SDS-PAGE and western blotting.

Western blotting was used to examine potential compensatory changes in striatal Orai or STIM expression in TRPC1$^{-/-}$ mice. These experiments were performed with striatal lysates prepared from 6 months and 12 months old WT and TRPC1$^{-/-}$ mice. Striata were dissected and homogenized by trituration in lysis buffer (100μl/striatum) containing (in mM): 137 NaCl, 2.7 KCl, 4.3 Na2HPO4, 1.4 KH2PO4, pH 7.2, 5 EDTA, 5 EGTA, 1 PMSF, 50 NaF, 1 Na3VO4 plus protease inhibitors, and 1% CHAPS. Samples were rotated for 1 hour at 4°C to solubilize proteins then centrifuged at 13000g for 10min. The supernatant was collected and the protein concentration was measuring using a NanoDrop (ThermoFisher Scientific). 6X SDS sample buffer was added to each sample to achieve a 1X concentration and then samples were diluted as appropriate with 1X SDS sample buffer to normalize the protein concentration of all samples. Samples were heated for 3min at 90°C and analyzed by SDS-PAGE and western blotting.

CRISPR/Cas9-mediated deletion of SOCE components

To delete neuronal SOC channels in corticostriatal co-cultures we used the CRISPR/Cas9 system. GuideRNA sequences targeting mouse TRPC4–6 and Orai1–2 were designed using bioinformatics tools (crispr.mit.edu for maximizing specificity and https://portals.broadinstitute.org/gpp/public/ for selecting guide sequences with predicted efficacy) and sgRNA plasmids targeting TRPC4–6 and Orai1–2 were generated. The sgRNA sequences for TRPC4 (5'-GAGGAGGGCGGTCCTTCCCAG-3'), TRPC5 (5'-GCATCCCCCTCCAAATCGTGA-3'), TRPC6 (5'-GAGCCAGGACTATTTGCTGA-3'), Orai1 (5'- GATCGGCCAGAGTTACTCCG-3') and Orai2 (5'GCTCAGGTAGAGCTTCCTCC-3') were subcloned into the lentiGuide-Puro plasmid (addgene.org/52963/) as in [32] following their protocol (https://media.addgene.org/data/plasmids/52/52963/52963-attachment_IPB7ZL_hJcbm.pdf). The lenti-Cas9-Blast plasmid (addgene.org/52962/) was used to express Cas9. As in [33], a guideRNA sequence (5'-GTGCGAATACGCCCACGCGAT-3') targeting the bacterial gene β-galactosidase (LacZ) was used as a negative control (gLacZ). Corticostriatal co-cultures were co-infected with lenti-Cas9 and lenti-sgRNA as previously described [13]. Western blotting as described above was used to analyze Cas9-mediated deletion in one to four batches of corticostriatal co-cultures.

Dendritic spine analysis of MSNs in primary corticostriatal co-cultures

Dendritic spine quantification was performed as previously described [22]. Corticostriatal co-cultures were established from WT, YAC128, TRPC1$^{-/-}$ and YAC128$^{+/-}$TRPC1$^{-/-}$ littermates to study the dendritic spines of MSNs. Briefly, striata and cortices were dissected from postnatal day 0–1 pups (in 1×HBSS, 16.36mM HEPES, 10mM $NaHCO_3$, 1× penicillin-streptomycin) digested with papain (30min at 37°C; Worthington), rinsed (Neurobasal-A medium with 10% FBS), dissociated (in dissection media with 5mg/ml DNaseI), and plated on poly-d-lysine coated 12mm coverslips in Neurobasal-A medium supplemented with 5% FBS, 2% B27 and 0.5mM l-glutamine (Invitrogen) and maintained at

37°C in a 5% CO_2 incubator, feeding weekly by addition of 400μl of NBA, 2% B27, and 0.5mM-glutamine. Cortices from one hemisphere and striata from three brains were used to plate 24 wells of a 24-well plate. We estimated that, on average, the resulting plating densities were 350 cells/mm^2 for cortical neurons (Ctx) and 1060 cells/mm^2 for MSNs, resulting in a 3:1 MSN:Ctx ratio [22]. Lentiviral particles were added on DIV7 to knockdown the target proteins.

For assessment of spine morphology, on DIV 20 corticostriatal co-cultures were fixed for 30min in 4% formaldehyde plus 4% sucrose in PBS, pH 7.4, and permeabilized for 5min in 0.25% Triton X-100. Fixed MSNs were blocked with 5% BSA in PBS and immunostained using a rabbit anti-DARPP-32 anti-body (1:500;Cell Signaling Technology,2306s) and a goat anti-rabbit Alexa Fluor 488 secondary antibody (1:1000) or a goat anti-rabbit Alexa Fluor 594 secondary antibody (1:1000). Z-stacks were captured using a 100×oil objective [Plan-Neofluor, 1.3 numerical aperture (NA)] with a confocal miscroscope (LSM510 Meta) with the pinhole set to one airy unit and optical sections every 0.3μm in Z. Dendritic spine density was quantified using NeuronStudio software in at least three batches of cultures for each experiment.

GCaMP5G Ca^{2+}-imaging experiments

GCaMP5G Ca^{2+}-imaging experiments were performed as described previously [34]. The corticostriatal co-cultures were prepared slightly different from the above method. The cortical cells were plated on DIV0 and infected with lenti-Cherry. After 24h, the medium was replaced with fresh medium and striatal cells were plated on DIV1. The WT, YAC128, $TRPC1^{-/-}$ and$YAC128^{+/-}TRPC1^{-/-}$ neurons were transfected with a GCaMP5G plasmid or a mixture of GCaMP5G and shRNAi plasmids (1:3 ratio) using a high calcium-phosphate transfection method [35] at DIV7 (CalPhos Transfection Kit; Clontech). MSNs in the co-culture were identified by GCaMP5G expression, morphology, and the lack of Cherry expression as in Wu et al., (2016). GCaMP5G fluorescent images were collected using an Olympus IX70 inverted epi-fluorescence microscope equipped with a 60×lens, Cascade 650 digital camera (Roper Scientific) and Prior Lumen 200 illuminator. Images from 488nm excitation were collected at 0.5Hz using MetaFluor (Universal Imaging). To measure synaptic nSOC, the neurons were incubated in Ca^{2+}-free medium (supplemented with 400 μM EGTA) containing 1μM thapsigargin (Tg) for 5min before returning to the ACSF containing 2mM Ca^{2+}, 1μM Tg and a Ca^{2+} channel inhibitor mixture (1μM TTX, 50μM AP5, 10 μM CNQX, and 50 μM nifedipine).The basal calcium level (F_0) in Ca^{2+}-free medium was recorded for ~40s before the addition of 2mM Ca^{2+} (F=the peak response to Ca^{2+} readdition). Data analysis was performed using ImageJ.

Motor coordination assessments in mice

Acohortof14WT,14YAC128,11$TRPC1^{-/-}$and 11 $YAC128^{+/-}TRPC1^{-/-}$ female littermates was used for behavioral studies. The motor coordination experiments were performed as previously described [21, 36]. The beam walking assay was carried out using a home-made experimental setup. A 17mm round plastic beam, 11mm round plastic beam, and 5mm square wood beam were used in our studies. At each time point, the mice were trained on beams for 3 consecutive days (3 trials/d) to traverse the beam to an enclosed box. Once the

stable baseline of performance was obtained, the mice were tested in three consecutive trials on 17 and 11mm round plastic beams and the 5mm square wood beam, in each case progressing from the widest to the narrowest beam. The latency to traverse the middle 80 cm of each beam and the number of times the hind feet slipped off each beam were recorded for each trial. For each measurement, the mean scores of the three trials for each beam were used in the analysis.

Dendritic spine analysis in mouse striatum

To establish a quantitative in vivo analysis of MSN spines, we adopted a procedure developed by [37]. WT, YAC128, TRPC1$^{-/-}$ and YAC128$^{+/-}$ TRPC1$^{-/-}$ mice at the age of 14 months were perfused intracardially with 5ml of ice-cold 1% paraformaldehyde (PFA) solution in 0.1M phosphate buffer (PB), followed by 60ml of 4% PFA plus 0.0625% glutaraldehyde in 0.1M PB over 12 min. Brains were removed and postfixed (4%PFA, 0.0625% glutaraldehyde, 0.1M PB) for 4h at 4°C. Fixed brains were coronally sliced (300μm sections) using a vibratome (Leica 1200S) and stored at 4°C in PBS with 0.05% NaN_3. Slices were mounted on a patch-clamp setup (Olympus BX51 microscope with an infrared camera portal). Glass electrodes for dye injection were pulled (150–300MΩ; Sutter Instruments P97) and striatal neurons were randomly injected and filled with Lucifer yellow solution (L-12926; Invitrogen). A constant negative current in the range of 1–3nA promoted dye infusion. MSN spines were imaged using a two-photon microscope (Zeiss LSM780) with a 40 × lens and 5 × zoom. MSNs were identified by their characteristic shape and abundance of spines as in Wu et al., 2016. For each neuron, a dendritic segment spaced at least 50μm from the soma or after the first branching point was considered for analysis. The spine density was analyzed using NeuronStudio software as described previously [22, 34].

Statistical analysis

The results are presented as mean±SEM (n=number of neurons or mice as indicated). Statistical comparisons of results obtained in experiments were performed by a Student's t test for two-group comparisons or a one-way or two-way ANOVA followed by Tukey's test for more than two comparisons among conditions. The multiplicity adjusted p value is reported as $p>0.05$=n.s, $p<0.05$=*, $p<0.01$=**, $p<0.001$=*** and $p<0.0001$=****.

RESULTS

Molecular composition of nSOC in MSNs

STIM, Orai and TRPC isoforms are broadly expressed in murine and human tissues including the brain [27, 28]. Previously we analyzed the neuronal expression of SOCE mediators using quantitative reverse transcription PCR (qRT-PCR) and found that STIM2, TRPC6, Orai2 and TRPC4 are enriched in the hippocampus of 8-week-old male C57BL/6 mice [38]. In contrast, none of these proteins are particularly enriched in the striatum relative to other brain regions, consistent with previous studies [39]. In our previous work, we demonstrated that knockdown or knockout of STIM2 rescues spine loss in YAC128 MSNs [22]. In hippocampal mushroom spines, Orai2 and TRPC6 mediate STIM2-gated nSOC [38]. Do any of these components mediate nSOC in MSNs? If so, do they contribute to spine loss in YAC128MSNs?

To answer these questions, we infected WT and YAC128 corticostriatal co-cultures with lentiviruses encoding siRNA targeting members of TRPC and Orai gene families. The spine morphology in infected cultures was evaluated by DARPP32-immunostaining and confocal imaging. TRPC2 was not examined, as it is a pseudogene in humans but is expressed in other species in a restricted pattern [40]. Western blots confirmed that siRNA reduced relevant protein targets (Fig. 1A). Compared to the siRNA control, expression was reduced from 1 to 0.57±0.089 for TRPC1, 0.68±0.019 for TRPC3, 0.11±0.0057 for TRPC4, 0.38±0.067 for TRPC5, 0.52±0.031 for TRPC6, 0.53±0.0017 for Orai1, 0.46±0.094 for Orai2 and 0.27±0.082 for STIM1 (n=2 for all samples). TRPC7 and Orai3 antibodies were not available to us. Consistent with our previous studies [13, 22], there was a substantial reduction in the density of MSN spines on DIV 20 from 12.0±0.3 spines/10μm (n=10) in WT co-cultures to 7.3±0.4 spines/10μm (n=10) in YAC128 co-cultures (Fig. 1B, C). The spine density of WT MSNs decreased significantly after knockdown of TRPC3, TRPC4 or TRPC5 (Fig. 1B, C). This indicates that TRPC3, TRPC4 and TRPC5 are necessary for WT MSN spine stability. Knockdown of these subunits did not rescue spine density in YAC128 MSNs (Fig. 1B, C). In contrast, knockdown of TRPC1 or TRPC6 had no effect on WT MSN spines but rescued the loss of spines in YAC128 MSNs. After knock down of TRPC1 the spine density in YAC128 MSNs was 13.0±1.0 spines/10 μm (n=10) and after knockdown of TRPC6 the spine density in YAC128 MSNs was 12.4±0.3 spines/10μm (n=10) (Fig. 1B, C). Knockdown of TRPC7 or Orai3 had no effect on spine density in WT and YAC128 MSNs (Fig. 1B, C). Knockdown of Orai1, Orai2 or STIM1 rescued the spine loss in YAC128 MSNs, increasing spine densityto11.4±1.1 spines/10 μm (n=10), 9.8±1.0 spines/10 μm (n=10) or 14.3±0.4 spines/10 (n=10), respectively (Fig. 1B, C).

To validate these findings we used lentiviral-delivered Cas9 and single guide RNA to disrupt expression of candidate nSOC channels by CRISPR/Cas9. Western blots confirmed that Cas9 reduced each protein target (Fig. 1D). Compared to the gLacZ control, expression was reduced from 1 to 0.19 for TRPC4 (n=1), 0.57±0.071 for TRPC5 (n=2), 0.43±0.069 for TRPC6 (n=3), 0.50±0.0052 for Orai1 (n=3) and 0.47±0.10 for Orai2 (n=4). In agreement with RNAi data, deletion of TRPC4 or TRPC5 genes reduced the WT MSN spine density and did not rescue the YAC128 MSN spine density (Fig. 1E, F). Also consistent with RNAi results, deletion of TRPC6, Orai1 or Orai2 had no effect on WT MSN spines but rescued the density of YAC MSN spines (Fig. 1E, F). We used TRPC1 knockout mice to further examine the viability of TRPC1 as a target (results presented later).

Results obtained in these experiments and in our previous studies [22] suggest that STIM1/2, TRPC1/6 and Orai1/2 can support supranormal nSOC in YAC128 MSNs. To test this hypothesis, we measured the amplitude of nSOC in WT and YAC128 MSN spines following knockdown of nSOC channel components. We focused on TRPC1, TRPC6, Orai1, and Orai2 because spine rescue data suggested that these proteins are potential therapeutic targets. We also tested the contribution of STIM1 to spine nSOC. To image calcium in MSN spines, we transfected a GCaMP5G plasmid into WT and YAC128 co-cultures [22, 34]. RNAi-mediated knockdown of TRPC1, TRPC6, Orai1, Orai2 or STIM1 significantly reduced spine SOC in both WT and YAC128 MSNs (Fig. 2A, B). These results suggest that both STIM1 and STIM2 [22] gate nSOC channel components in MSNs, which may include TRPC1, TRPC6, Orai1 and Orai2.

In the next series of experiments, we used a biochemical approach to test whether STIM1 and/or STIM2 physically interact with TRPC and Orai channels in the striatum. We prepared striatal synaptosomes and performed a series of co-immunoprecipitation experiments. We found that antibodies Against Orai1 or Orai2 efficiently pulled down STIM1 and STIM2 from striatal synaptosomal lysates (Fig. 3). We also observed association of STIM1 and STIM2 with TRPC1 and TRPC6 subunits (Fig. 3). No signal was observed in TRPC4 immunoprecipitation experiments (Fig. 3) and also no signal was observed in immunoprecipitation experiments with TRPC3 and TRPC5 antibodies (data not shown). Overall, these data are consistent with the involvement of TRPC1, TRPC6, Orai1, Orai2, STIM1 and STIM2 in spine nSOC in striatal MSNs.

Knockout of TRPC1 rescues spine loss and suppresses spine nSOC in YAC128 MSNs

In previous studies we demonstrated that knockdown of STIM2, TRPC6, or Orai2 proteins causes loss of mushroom spines in hippocampal neurons [34, 38], making them not suitable targets for non-localized HD treatments. STIM1 and Orai1 are also not ideal for systemic suppression, as mutations in them are associated with immunodeficiency in human patients [41]. STIM1$^{-/-}$ mice perish *in utero* or soon after birth from respiratory failure, although early embryos appeared to develop normally [42]. Orai1$^{-/-}$ mice suffer from immune deficits and other detrimental phenotypes [43]. By contrast, the phenotype of TRPC1$^{-/-}$ mice is relatively mild [30], suggesting that TRPC1 may be a better target for suppressing hyperactive nSOC in YAC128 MSNs. We therefore used TRPC1$^{-/-}$ mice to further investigate the role of TRPC1 in YAC128 MSN nSOC and spineinstability.FortheseexperimentsYAC128mice were crossed with TRPC1$^{-/-}$ mice [30] to generate YAC128$^{+/-}$ TRPC1$^{-/-}$ mice.

In our experiments corticostriatal co-cultures were established from WT, YAC128, TRPC1$^{-/-}$ and YAC128$^{+/-}$ TRPC1$^{-/-}$ mice. As commercial TRPC1 antibodies are unable to detect the absence of TRPC1 protein in TRPC1 knockout mice [44], we used qPCR and RT-PCR to confirm that exon 8 of TRPC1, which encodes transmembrane domains 4 and 5 as well as part of the pore region [45], was absent from striatal transcripts of TRPC1$^{-/-}$ and YAC128$^{-/-}$ TRPC1$^{-/-}$ mice. TRPC1 message was not detectable by qPCR or visible when RT-PCR products were analyzed by gel electrophoresis in TRPC1$^{-/-}$ and YAC128$^{+/-}$ TRPC1$^{-/-}$ samples (Fig. 4A), confirming the knockout. Striatal lysates from WT and TRPC1$^{-/-}$ mice (6 and 12 months of age) were analyzed by western blotting to check for compensatory changes in Orai or STIM expression. Example blots are shown in Fig. 4B. We did not observe any significant differences in expression levels of STIM and Orai isoforms between WT and TRPC1$^{-/-}$ mice (n=4 for WT mice at 6 months; n=4 for TRPC1$^{-/-}$ mice at 6 months; n=4 for WT mice at 12 months; n=2 for TRPC1$^{-/-}$ mice at 12 months). GCaMP5G was transfected into these cultures to measure nSOC in the spines of WT, YAC128, TRPC1$^{-/-}$ and YAC128$^{+/-}$TRPC1$^{-/-}$MSNs. Spine nSOC was significantly decreased in TRPC1$^{-/-}$ and YAC128$^{+/-}$TRPC1$^{-/-}$ MSNs when compared with WT and YAC128 MSNs, respectively (Fig. 4C, D). This is consistent with results from TRPC1 RNAi knockdown Ca^{2+} imaging experiments (Fig. 2A, B) and with the decreased SOC observed in submandibular gland acini and ductal cells prepared from TRPC1$^{-/-}$ mice [30]. We evaluated spine morphology of striatal MSNs in corticostriatal co-cultures from WT,

YAC128$^{+/-}$, TRPC1$^{-/-}$ and YAC128$^{+/-}$TRPC1$^{-/-}$ mice by DARPP32 immunostaining and confocal imaging. On average, the density of WT MSN spines was equal to 11.8±0.7 spines/10μm of dendritic length (n=10) and the density of YAC128 MSN spines was equal to 7.2±0.4 spines/10μm (n=10) (Fig. 4E, F). There was no difference in spine density between TRPC1$^{-/-}$ and WT MSNs (Fig. 4E, F). The spine density of YAC128$^{+/-}$TRPC1$^{-/-}$ MSNs was 14.7±0.5 spines/10μm (n=10) (Fig. 4E, F), significantly increased when compared to YAC128 MSNs. These data are consistent with TRPC1 RNAi knock-down experiments (Fig. 1B, C). Our results suggest that knocking out TRPC1 is synaptoprotective for YAC128 MSNs *in vitro*. Does the absence of TRPC1 rescue motor deficits and spine loss in YAC128 mice *in vivo*?

Knockout of TRPC1 improves motor coordination and prevents spine loss in YAC128 mice

Expression of YAC128 transgene or knockout of TRPC1 resulted in elevation of body weight in these mutant mice (Fig. 5A). The weight of YAC128$^{+/-}$TRPC1$^{-/-}$ mice increased even faster than for YAC128$^{+/-}$ or TRPC1$^{-/-}$ mice (Fig. 5A). At the age of 9.5 months, the average weight of YAC128$^{+/-}$TRPC1$^{-/-}$ mice was 51.6±1.7g, 22% more than the weight of YAC128$^{+/-}$ mice and 66% more than the weight of WT mice (Fig. 5A). In previous studies we used 5 mm square, 11 mm round and 17 mm round beams to quantify motor impairment of YAC128 mice in a beamwalk assay [21, 36, 46, 47]. However, the excessive body weight of YAC128$^{+/-}$TRPC1$^{-/-}$ mice appeared to cause their reluctance to walk on the 11 mm or 5 mm beams. Therefore the 17 mm beam was used for all groups and ages. All 4 groups of mice were trained to walk across 17 mm beam to reach an enclosed box, and the time to traverse the beam and the number of foot slips while walking on the beam was recorded for each trial. In this assay we found that the beamwalk performance of all 4 groups of mice was similar at 1.5,4.5 and 6.5 months of age (Fig. 5B,C).Consistent with our previous studies, aging YAC128 mice exhibited progressive impairment in beam walking ability when compared to WT mice [21]. At 9.5 months and 12 months of age the beam crossing duration was significantly longer for YAC128 mice (Fig. 5B) and they had a significantly increased number of foot slips when compared to WT mice (Fig. 5C). TRPC1$^{-/-}$ mice exhibited similar behavior as WT mice from 1.5 months to 9.5 months of age. At 12 month of age, TRPC1$^{-/-}$ mice showed a motor deficit compared to WT mice (Fig. 5B, C), but it was not as severe as the deficit in YAC128 mice. These findings are consistent with a previous analysis showing a delayed motor deficit in TRPC1$^{-/-}$ mice [48]. YAC128$^{+/-}$TRPC1$^{-/-}$ mice exhibited significantly decreased beam crossing latencies and fewer foot slips when compared with YAC128 mice at 9.5 months and 12 months of age (Fig. 5B,C).The performance of YAC128$^{+/-}$TRPC1$^{-/-}$ mice was identical to the performance of TRPC1$^{-/-}$ mice at all ages tested (Fig. 5B, C). Based on these results, we concluded that knocking out TRPC1 mitigates the motor coordination deficit in YAC128 mice.

Following conclusion of behavioral tests, all 4 groups of mice were anesthetized, exsanguinated and perfused with fixative at 14 months of age. The brains were post-fixed, coronally sliced at 300μm and the striatal MSNs were microinjected with the fluorescent dye Lucifer yellow [37].Analys is of spine morphology was performed by two-photon imaging of the injected striatal sections. In agreement with the previous results [22], we observed a significant reduction in the MSN spine density in 14 months old YAC128$^{+/-}$ mice when

compared with WT mice (Fig. 6A, B). On average, the MSN spine density was reduced from 16.9 ± 0.4 spines/10μm dendritic length (n=65 neurons from 10 mice) in WT mice to 11.2 ± 0.2 spines/10μm (n=101 neurons from 13 mice; p<0.001) in YAC128$^{+/-}$ mice (Fig. 6B). The MSN spine density in TRPC1$^{-/-}$ mice was 16.1 ± 0.5 spines/10μm (n=47 neurons from 9 mice), the same as in WT mice (Fig. 6A, B). Deletion of TRPC1 gene rescued spine loss in YAC128$^{+/-}$TRPC1$^{-/-}$ mice, resulting in a spine density equal to 16.5 ± 0.4 spines/10μm (n=48 neurons from 8 mice) (Fig. 6A, B). Compared to YAC128$^{+/-}$ MSNs, YAC128$^{+/-}$TRPC1$^{-/-}$ MSNs had a significantly increased spine density (Fig. 6B). These results confirm that knocking out TRPC1 helps to stabilize MSN spines in YAC128 HD mice *in vivo*.

DISCUSSION

TRPC1 as a potential therapeutic target for Huntington's disease

Store-operated Ca^{2+} entry (SOC) plays an important role in non-excitable cells, in particular in cells from immune system. The functional role and properties of neuronal SOC (nSOC) are much less clear. nSOC is thought by some as redundant or even unnecessary, as there are numerous kinds of Ca^{2+}-conducting channels in neurons [49].However,recent evidence implicates nSOC in the regulation of neuronal functions and there is a growing interest in characterizing properties of nSOC [27, 34, 50–52]. In non-excitable cells, the molecular composition of SOC pathway includes the ER Ca^{2+} sensors STIM1 and STIM2, as well as the store-operated Ca^{2+}-channels from Orai and TRPC families [24]. STIM1 and STIM2 proteins are expressed in neurons, with STIM2 most abundantly expressed in the hippocampus and STIM1 in the cerebellar Purkinje cells. It has been demonstrated that STIM1 and STIM2 mediate nSOC in neurons [38, 53–58]. Orai1, Orai2 and Orai3 proteins are expressed in neurons. The role of Orai1 and Orai2 proteins in supporting nSOC was documented [38, 55]. Both STIM1 and STIM2 were implicated in the control of Orai channel activity in neurons [38, 55, 57]. TRPC channels are also expressed in neurons and may contribute to nSOC [26, 27, 38, 50, 59]. Different members of the TRPC family play important signaling functions in neurons [25,60] and it has been suggested that neuronal TRPC channels constitute potential therapeutic targets for treating neurodegenerative disorders and other disorders of the nervous system [28, 61].

In our previous studies we identified enhanced nSOC as one of the potential causes of synaptic and neuronal loss in HD [22,23].We found in an unbiased screen that a novel class of nSOC inhibitors improved motor performance in HD flies and observed excessive nSOC in MSNs from the YAC128 transgenic mouse model of HD [23]. Similar enhancement of nSOC was reported in studies with cultured cells transfected with a plasmid encoding the exon 1 fragment of mHtt [62]. We further demonstrated the presence of enhanced nSOC in synaptic spines of YAC128 MSNs and determined that STIM2 knock-down or knockout rescued the spine loss phenotype in YAC128 MSNs [22]. In the present study we set out to identify additional molecular components of nSOC which can be targeted for therapeutic interventions. We performed a systematic knockdown of TRPC and Orai family members and analyzed resulting effects on the density of MSN spines in wild type corticostriatal co-cultures and in cultures from YAC128 HD mice. We found that knockdown of TRPC1,

TRPC6, Orai1, Orai2 or STIM1, but not any other member of the TRPC family or Orai3, was able to rescue spine loss in YAC128 MSNs without affecting the spine density of wild type MSNs (Fig. 1B, C). This result was recapitulated by deleting TRPC6,Orai1,or Orai2 using Cas9 (Fig. 1E, F) and by preparing cultures from TRPC1 knockout mice (Fig. 4). Knockdown of TRPC1, TRPC6, Orai1, Orai2 or STIM1, suppresses spine nSOC in YAC128 MSNs (Fig. 2). In addition to STIM2 [22], these results suggest that TRPC1, TRPC6, Orai1, Orai2 and STIM1 all contribute to supranormal nSOC in YAC128 MSN spines.

It is important to note that the density of WT MSN spines was not affected by reduced spine nSOC levels (Fig. 2) from knockdown of TRPC1, TRPC6, Orai1, Orai2 or STIM1 (Fig. 1). Likewise, WT MSN spine prevalence was unaffected by knockdown of $InsP_3R1$, a manipulation that lowers spine nSOC [22]. However, knockdown of STIM2 resulted in a partial loss of WT MSN spines [22]. As nSOC reduction (Fig. 2) is generally insufficient to decrease the density of WT MSN spines (Fig.1), STIM2 may have a pleiotropic role in regulating MSN spine integrity that is independent of SOC. For example, perhaps STIM2 dynamically remodels the ER [63], a process that could impact synaptic plasticity [64]. In contrast to spines of MSNs, stability of mushroom spines of hippocampal neurons requires nSOC [34]. Thus, different populations of neurons maintain spines though distinct mechanisms that are not fully understood.

In biochemical experiments, we observed an association of endogenous STIM1 or STIM2 with TRPC1, TRPC6, Orai1 and Orai2, but not TRPC3, TRPC4 or TRPC5 in synaptosomal lysates from WT striata (Fig. 3 and data not shown). This further supports the role of these channels in the regulation of nSOC in MSN spines, as the channels that contribute to spine loss and nSOC in YAC MSNs more strongly interacted with STIM1/2. STIM1/2 binding to Orai1/2 is likely direct, whereas TRPC1/6 may interface with Orai channels to augment signaling [40]. Alternatively, TRPC1 was reported to directly interact with STIM1, but STIM1 may indirectly regulate TRPC6 via STIM1-dependent regulation of heteromultimerization [65]. TRPC1 dynamically interacts with STIM1 and Orai1 in response to store depletion and a TRPC1/STIM1/Orai1 complex was observed in human salivary gland cells [66], mouse pulmonary arterial smooth muscle cells [67] and rat kidney fibroblasts [68]. Also, TRPC6/STIM1/Orai1 association was observed in human platelets [69]. Knockdown of any of these SOC components can rescue the spine loss of YAC128 MSNs. This indicates that these components are not functionally redundant, but rather they cooperate to mediate nSOC.

We focused on TRPC1 as a potential therapeutic target. Role of TRPC1 in supporting supranormal nSOC in YAC128 MSNs was also supported by the previous studies [23, 62]. The phenotype of $TRPC1^{-/-}$ mice is relatively mild [30]. In the present study, we crossed $TRPC1^{-/-}$ mice with the YAC128 mice to further evaluate the role of TRPC1 in MSN spine nSOC. Genetic ablation of TRPC1 was associated with suppression of nSOC and prevented YAC128 MSN spine loss *in vitro* (Fig. 4). nSOC was partially attenuated in WT MSNs lacking TRPC1, indicating that it contributes to non-pathological nSOC as well. We evaluated motor performance of WT, YAC128, $TRPC1^{-/-}$ and $YAC128^{+/-}TRPC1^{-/-}$ mice using the beamwalk assay (Fig. 5). Knocking out TRPC1 had no effect on motor performance until after 9.5 months of age, in agreement with delayed motor deficits

previously reported for TRPC1$^{-/-}$ mice [48]. However, deletion of TRPC1 in YAC128 mice improved their motor performance relative to YAC128 mice to levels that were comparable to TRPC1$^{-/-}$ mice. This indicates that TRPC1 contributes to the development of motor symptoms in YAC128 mice. We also established that knockout of TRPC1 prevented the loss of MSN spines in YAC128 mice *in vivo* (Fig. 6), confirming a critical role for TRPC1 in synaptic loss in the YAC128 model of HD. From these studies we concluded that TRPC1 is a potential therapeutic target for treatment of HD.

Our data suggests that the rescue of YAC128 MSN spines relates to reducing nSOC below synaptotoxic levels, but we cannot rule out additional mechanisms. For example, it has been reported that glutamate activates cell death by massive influx of Ca^{2}+ via the TRPC1 channel [70]. They reported that TRPC1 expression was increased after glutamate treatment and that blockade of TRPC1 significantly reduces cell death in hippocampal organotypic slice cultures. Potential limitations of TRPC1 as a target involve its function in other brain regions. Reduced nSOC was recently demonstrated to be linked with the loss of substantia nigra neurons in Parkinson's disease (PD) [71]. TRPC1 knockout mice exhibit a spatial memory deficit [72], reduced activity in swimming and locomotion and some neuronal loss in basal ganglia and substantia nigra [48, 73]. Enhanced expression of TRPC1 resulted in neuroprotective effects in cellular models of PD [73–76]. These results suggest that the therapeutic window for TRPC1 inhibitors in HD maybe limited by detrimental effects of these inhibitors in substantia nigra dopaminergic neurons. TRPC1 was also identified as a mediator of postsynaptic Ca^{2}+ influx required for BDNF-induced synaptic plasticity at the developing neuromuscular junction [77].

Our data suggest that aberrant calcium signals mediated by TRPC1 and possibly other nSOC channel subunits (TRPC6, Orai1 and Orai2) leads to synaptic and motor pathology in the YAC128 mouse model of HD. We conclude that TRPC1 could be a suitable neuroprotective target for treatment of HD. The therapeutic window for TRPC1 inhibitors in HD maybe limited by potential detrimental effects of these inhibitors in substantia nigra dopaminergic neurons.

ACKNOWLEDGMENTS

We thank Leah Taylor for administrative assistance, Anna Starokadomska for technical assistance with cloning, Xia Liang for assistance with behavioral studies. The research described herein was supported by the National Institute of Neurological Disorders and Stroke of the National Institutes of Health (R01NS074376 and R01NS056224, IB; F32NS093786, DAR) and by the NIH Intramural Research Program (project Z01-ES-101684 to LB). IB holds the Carl J. and Hortense M. Thomsen Chair in Alzheimer's Disease Research.

REFERENCES

[1]. The Huntington's Disease Collaborative Research Group. A novel gene containing a trinucleotide repeat that is expanded and unstable on Huntington's disease chromosomes. Cell. 1993;72(6): 971–83. [PubMed: 8458085]

[2]. Vonsattel JP, Myers RH, Stevens TJ, Ferrante RJ, Bird ED, Richardson EP, Jr. Neuropathological classification of Huntington's disease. J Neuropathol Exp Neurol. 1985;44(6): 559–77. [PubMed: 2932539]

[3]. Rosas H, Koroshetz W, Chen Y, Skeuse C, Vangel M, Cudkowicz M, et al. Evidence for more widespread cerebral pathology in early HD: An MRI-based morphometric analysis. Neurology. 2003;60(10):1615–20. [PubMed: 12771251]

[4]. Zuccato C, Valenza M, Cattaneo E. Molecular mechanisms and potential therapeutical targets in Huntington's disease. Physiol Rev. 2010;90(3):905–81. [PubMed: 20664076]

[5]. Miller BR, Bezprozvanny I. Corticostriatal circuit dysfunction in Huntington's disease: Intersection of glutamate, dopamine, and calcium. Future Neurol. 2010;5:735–56. [PubMed: 21977007]

[6]. Bunner KD, Rebec GV. Corticostriatal dysfunction in Huntington's disease: The basics. Front Hum Neurosci. 2016;10:317. [PubMed: 27445757]

[7]. Milnerwood AJ, Raymond LA. Early synaptic pathophysiology in neurodegeneration: Insights from Huntington's disease. Trends Neurosci. 2010;33(11):513–23. [PubMed: 20850189]

[8]. Galvan L, Andre VM, Wang EA, Cepeda C, Levine MS. Functional differences between direct and indirect striatal output pathways in Huntington's disease.J Huntingtons Dis. 2012;1(1):17–25. [PubMed: 25063187]

[9]. Plotkin JL, Surmeier DJ. Corticostriatal synaptic adaptations in Huntington's disease. Curr Opin Neurobiol. 2015;33:53–62. [PubMed: 25700146]

[10]. Wyant KJ, Ridder AJ, Dayalu P. Huntington's diseaseupdate on treatments. Curr Neurol Neurosci Rep.2017;17(4):33. [PubMed: 28324302]

[11]. Shannon KM, Fraint A. Therapeutic advances in Huntington's disease. Mov Disord. 2015;30(11): 1539–46. [PubMed: 26226924]

[12]. McColgan P, Tabrizi SJ. Huntington's disease: A clinical review. Eur J Neurol. 2018;25(1):24–34. [PubMed: 28817209]

[13]. Ryskamp D, Wu J, Geva M, Kusko R, Grossman I, Hayden M, et al.The sigma-1 receptor mediates the beneficial effects of pridopidine in a mouse model of Huntington disease. Neurobiol Dis. 2017;97:46–59. [PubMed: 27818324]

[14]. de Yebenes JG, Landwehrmeyer B, Squitieri F, Reilmann R, Rosser A, Barker RA, et al. Pridopidine for the treatment of motor function in patients with Huntington's disease (MermaiHD): A phase 3, randomised, double-blind, placebo-controlled trial. Lancet Neurol. 2011;10(12): 1049–57. [PubMed: 22071279]

[15]. Huntington Study Group HART Investigators. A randomized, double-blind, placebo-controlled trial of pridopidine in Huntington's disease. Mov Disord. 2013;28(10): 1407–15. [PubMed: 23450660]

[16]. Kieburtz K, Landwehrmeyer GB, Reilmann R, Savola J, Eyal E, Grachev I, et al. Efficacy, safety, and tolerability of pridopidine in Huntington disease (HD): Results from the phase II, double-blind, placebo-controlled, dose-ranging study, Pride-HD (P2. 005). Neurology. 2017;88(16 Supplement):P2. 005.

[17]. McGarry A, Kieburtz K, Abler V, Grachev ID, Gandhi S, Auinger P, et al. Safety and exploratory efficacy at 36 months in Open-HART, an open-label extension study of pridopidine in Huntington's disease. J Huntingtons Dis. 2017;6(3):189–99. [PubMed: 28826192]

[18]. Tang TS, Tu H, Chan EY, Maximov A, Wang Z, Wellington CL, et al. Huntingtin and huntingtin-associated protein 1 influence neuronal calcium signaling mediated by inositol-(1,4,5) triphosphate receptor type 1. Neuron. 2003;39(2):227–39. [PubMed: 12873381]

[19]. Tang TS, Tu H, Orban PC, Chan EY, Hayden MR, Bezprozvanny I. HAP1 facilitates effects of mutant huntingtin on inositol 1,4,5-trisphosphate-induced Ca release in primary culture of striatal medium spiny neurons. Eur J Neurosci. 2004;20(7):1779–87. [PubMed: 15379999]

[20]. Tang TS, Slow E, Lupu V, Stavrovskaya IG, Sugimori M, Llinas R, et al. Disturbed Ca2+ signaling and apoptosis of medium spiny neurons in Huntington's disease. Proc Natl Acad Sci U S A. 2005;102(7):2602–7. [PubMed: 15695335]

[21]. Tang TS, Guo C, Wang H, Chen X, Bezprozvanny I. Neuroprotective effects of inositol 1,4,5-trisphosphate receptor C-terminal fragment in a Huntington's disease mouse model. J Neurosci. 2009;29(5):1257–66. [PubMed: 19193873]

[22]. Wu J, Ryskamp DA, Liang X, Egorova P, Zakharova O, Hung G, et al. Enhanced store-operated calcium entry leads to striatal synaptic loss in a Huntington's disease mouse model. J Neurosci. 2016;36(1):125–41. [PubMed: 26740655]

[23]. Wu J, Shih HP, Vigont V, Hrdlicka L, Diggins L, Singh C, et al. Neuronal store-operated calcium entry pathway as a novel therapeutic target for Huntington's disease treatment. Chem Biol. 2011;18(6):777–93. [PubMed: 21700213]

[24]. Prakriya M, Lewis RS. Store-operated calcium channels. Physiol Rev. 2015;95(4):1383–436. [PubMed: 26400989]

[25]. Zeng C, Tian F, Xiao B. TRPC channels: Prominent candidates of underlying mechanism in neuropsychiatric diseases. Mol Neurobiol. 2016;53(1):631–47. [PubMed: 25502458]

[26]. Moccia F, Zuccolo E, Soda T, Tanzi F, Guerra G, Mapelli L, et al. Stim and Orai proteins in neuronal Ca(2+) signaling and excitability. Front Cell Neurosci. 2015;9:153. [PubMed: 25964739]

[27]. Kraft R STIM and ORAI proteins in the nervous system. Channels. 2015;9(5):245–52. [PubMed: 26218135]

[28]. Selvaraj S, Sun Y, Singh BB. TRPC channels and their implication in neurological diseases. CNS Neurol Disord Drug Targets. 2010;9(1):94–104. [PubMed: 20201820]

[29]. Fisher A, Bezprozvanny I, Wu L, Ryskamp DA, Bar-Ner N, Natan N, et al. AF710B, a novel M1/σ1 agonist with therapeutic efficacy in animal models of Alzheimer's disease. Neurodegener Dis. 2016;16(1–2):95–110. [PubMed: 26606130]

[30]. Liu X, Cheng KT, Bandyopadhyay BC, Pani B, Dietrich A, Paria BC, et al. Attenuation of store-operated Ca2+ current impairs salivary gland fluid secretion in TRPC1(−/−) mice. Proc Natl Acad Sci U S A. 2007;104(44):17542–7. [PubMed: 17956991]

[31]. Slow EJ, van Raamsdonk J, Rogers D, Coleman SH, Graham RK, Deng Y, et al. Selective striatal neuronal loss in a YAC128 mouse model of Huntington disease. Hum Mol Genet. 2003;12(13): 1555–67. [PubMed: 12812983]

[32]. Sanjana NE, Shalem O, Zhang F. Improved vectors and genome-wide libraries for CRISPR screening. Nat Methods. 2014;11(8):783–4. [PubMed: 25075903]

[33]. Platt RJ, Chen S, Zhou Y, Yim MJ, Swiech L, Kempton HR, et al. CRISPR-Cas9 knockin mice for genome editing and cancer modeling. Cell. 2014;159(2):440–55. [PubMed: 25263330]

[34]. Sun S, Zhang H, Liu J, Popugaeva E, Xu NJ, Feske S, et al. Reduced synaptic STIM2 expression and impaired store-operated calcium entry cause destabilization of mature spines in mutant presenilin mice. Neuron. 2014;82(1):7993.

[35]. Jiang M, Chen G. High Ca2+-phosphate transfection efficiency in low-density neuronal cultures. Nat Protoc. 2006;1(2):695–700. [PubMed: 17406298]

[36]. Tang TS, Chen X, Liu J, Bezprozvanny I. Dopaminergic signaling and striatal neurodegeneration in Huntington's disease. J Neurosci. 2007;27(30):7899–910. [PubMed: 17652581]

[37]. Dumitriu D, Rodriguez A, Morrison JH. High-throughput, detailed, cell-specific neuroanatomy of dendritic spines using microinjection and confocal microscopy. Nat Protoc. 2011;6(9):1391–411. [PubMed: 21886104]

[38]. Zhang H, Sun S, Wu L, Pchitskaya E, Zakharova O, Fon Tacer K, et al. Store-operated calcium channel complex in postsynaptic spines: A new therapeutic target for Alzheimer's disease treatment. J Neurosci. 2016;36(47): 11837–50. [PubMed: 27881772]

[39]. Riccio A, Medhurst AD, Mattei C, Kelsell RE, Calver AR, Randall AD, et al. mRNA distribution analysis of human TRPC family in CNS and peripheral tissues. Brain Res Mol Brain Res. 2002;109(1–2):95–104. [PubMed: 12531519]

[40]. Cheng KT, Ong HL, Liu X, Ambudkar IS. Contribution and regulation of TRPC channels in store-operated Ca2+ entry. Curr Top Membr. 2013;71:149–79. [PubMed: 23890115]

[41]. Feske S CRAC channelopathies. PflugersArch. 2010;460(2):417–35.

[42]. Cahalan MD. STIMulating store-operated Ca2+ entry. Nat Cell Biol. 2009;11(6):669–77. [PubMed: 19488056]

[43]. Gwack Y, Srikanth S, Oh-Hora M, Hogan PG, Lamperti ED, Yamashita M, et al. Hair loss and defective T-and B-cell function in mice lacking ORAI1. Mol Cell Biol. 2008;28(17):5209–22. [PubMed: 18591248]

[44]. Dietrich A, Fahlbusch M, Gudermann T. Classical transient receptor potential 1 (TRPC1): Channel or channel regulator? Cells. 2014;3(4):939–62. [PubMed: 25268281]

[45]. Dietrich A, Kalwa H, Storch U, y Schnitzler MM, Salanova B, Pinkenburg O, et al. Pressure-induced and storeoperated cation influx in vascular smooth muscle cells is independent of TRPC1. Pflugers Arch. 2007;455(3): 465–77. [PubMed: 17647013]

[46]. Wang H, Chen X, Li Y, Tang TS, Bezprozvanny I. Tetrabenazine is neuroprotective in Huntington's disease mice. Mol Neurodegener. 2010;5:18. [PubMed: 20420689]

[47]. Liang X, Wu J, Egorova P, Bezprozvanny I. An automated and quantitative method to evaluate progression of striatal pathology in Huntington's disease transgenic mice. J Huntingtons Dis. 2014;3(4):343–50. [PubMed: 25575955]

[48]. He K, Qi F, Guo C, Zhan S, Xu H, Liu J, et al. Movement deficits and neuronal loss in basal ganglia in TRPC1 deficient mice. Oncotarget. 2016;7(43):69337. [PubMed: 27738307]

[49]. Lu B, Fivaz M. Neuronal SOCE: Myth or reality? Trends Cell Biol. 2016;26(12):890–3. [PubMed: 27720332]

[50]. Majewski L, Kuznicki J. SOCE in neurons: Signaling or just refilling? Biochim Biophys Acta. 2015;1853(9): 1940–52. [PubMed: 25646572]

[51]. Segal M, Korkotian E. Roles of calcium stores and store-operated channels in plasticity of dendritic spines. Neuroscientist. 2016;22(5):477–85. [PubMed: 26511041]

[52]. Popugaeva E, Pchitskaya E, Bezprozvanny I. Dysregulation of neuronal calcium homeostasis in Alzheimer's disease - A therapeutic opportunity? Biochem Biophys Res Commun. 2017;483(4): 998–1004. [PubMed: 27641664]

[53]. Berna-Erro A, Braun A, Kraft R, Kleinschnitz C, Schuhmann MK, Stegner D, et al. STIM2 regulates capacitive Ca2+ entry in neurons and plays a key role in hypoxic neuronal cell death. Sci Signal. 2009;2(93):ra67. [PubMed: 19843959]

[54]. Klejman ME, Gruszczynska-Biegala J, Skibinska-Kijek A, Wisniewska MB, Misztal K, Blazejczyk M, et al. Expression of STIM1 in brain and puncta-like co-localization of STIM1 and ORAI1 upon depletion of Ca(2+) store in neurons. Neurochem Int. 2009;54(1):49–55. [PubMed: 19013491]

[55]. Korkotian E, Oni-Biton E, Segal M. The role of the store-operated calcium entry channel Orai1 in cultured rat hippocampal synapse formation and plasticity. J Physiol. 2017;595(1):125–40. [PubMed: 27393042]

[56]. Gruszczynska-Biegala J, Pomorski P, Wisniewska MB, Kuznicki J. Differential roles for STIM1 and STIM2 in store-operated calcium entry in rat neurons. PLoS One. 2011;6(4):e19285. [PubMed: 21541286]

[57]. Gruszczynska-Biegala J, Kuznicki J. Native STIM2 and ORAI1 proteins form a calcium-sensitive and thapsigargininsensitive complex in cortical neurons. J Neurochem. 2013;126(6):727–38. [PubMed: 23711249]

[58]. Hartmann J, Karl RM, Alexander RP, Adelsberger H, Brill MS, Ruhlmann C, et al. STIM1 controls neuronal Ca(2)(+) signaling, mGluR1-dependent synaptic transmission, and cerebellar motor behavior. Neuron. 2014;82(3): 635–44. [PubMed: 24811382]

[59]. Strubing C, Krapivinsky G, Krapivinsky L, Clapham DE. TRPC1 and TRPC5 form a novel cation channel in mammalian brain. Neuron. 2001;29(3):645–55. [PubMed: 11301024]

[60]. Bollimuntha S, Selvaraj S, Singh BB. Emerging roles of canonical TRP channels in neuronal function. Adv Exp Med Biol. 2011;704:573–93. [PubMed: 21290317]

[61]. Wang Y, Bu J, Shen H, Li H, Wang Z, Chen G. Targeting transient receptor potential canonical channels for nervous system diseases. Curr Drug Targets. 2017;18(12): 1460–5. [PubMed: 26648074]

[62]. Vigont V, Kolobkova Y, Skopin A, Zimina O, Zenin V, Glushankova L, et al. Both Orai1 and TRPC1 are involved in excessive store-operated calcium entry in striatal neurons expressing mutant huntingtin exon 1. Front Physiol. 2015;6:337. [PubMed: 26635623]

[63]. Grigoriev I, Gouveia SM, Van der Vaart B, Demmers J, Smyth JT, Honnappa S, et al. STIM1 is a MT-plus-endtracking protein involved in remodeling of the ER. Curr Biol. 2008;18(3):177–82. [PubMed: 18249114]

[64]. Holbro N, Grunditz A, Oertner TG. Differential distribution of endoplasmic reticulum controls metabotropic signaling and plasticity at hippocampal synapses. Proc Natl Acad Sci U S A. 2009;106(35):15055–60. [PubMed: 19706463]

[65]. Yuan JP, Zeng W, Huang GN, Worley PF, Muallem S. STIM1 heteromultimerizes TRPC channels to determine their function as store-operated channels. Nat Cell Biol. 2007;9(6):636–45. [PubMed: 17486119]

[66]. Ong HL, Cheng KT, Liu X, Bandyopadhyay BC, Paria BC, Soboloff J, et al. Dynamic assembly of TRPC1-STIM1-Orai1 ternary complex is involved in store-operated calcium influx. Evidence for similarities in store-operated and calcium release-activated calcium channel components. J Biol Chem. 2007;282(12):9105–16. [PubMed: 17224452]

[67]. Ng LC, McCormack MD, Airey JA, Singer CA, Keller PS, Shen XM, et al. TRPC1 and STIM1 mediate capacitative Ca2+ entry in mouse pulmonary arterial smooth muscle cells. J Physiol. 2009;587(11):2429–42. [PubMed: 19332490]

[68]. Almirza W, Peters P, van Zoelen E, Theuvenet A. Role of Trpc channels, Stim1 and Orai1 in PGF 2α-induced calcium signaling in NRK fibroblasts. Cell Calcium. 2012;51(1):12–21. [PubMed: 22050845]

[69]. Jardin I, Gomez LJ, Salido GM, Rosado JA. Dynamic interaction of hTRPC6 with the Orai1-STIM1 complex or hTRPC3 mediates its role in capacitative or non-capacitative Ca(2+) entry pathways. Biochem J. 2009;420(2):267–76. [PubMed: 19260825]

[70]. Narayanan KL, Irmady K, Subramaniam S, Unsicker K, von Bohlen und Halbach O. Evidence that TRPC1 is involved in hippocampal glutamate-induced cell death. Neurosci Lett. 2008;446(2–3):117–22. [PubMed: 18822346]

[71]. Zhou Q, Yen A, Rymarczyk G, Asai H, Trengrove C, Aziz N, et al. Impairment of PARK14-dependent Ca(2+) signalling is a novel determinant of Parkinson's disease. Nat Commun. 2016;7:10332. [PubMed: 26755131]

[72]. Xing R, Zhang Y, Xu H, Luo X, Chang RC-C, Liu J, et al. Spatial memory impairment by TRPC1 depletion is ameliorated by environmental enrichment. Oncotarget. 2016;7(19):27855. [PubMed: 27034165]

[73]. Selvaraj S, Sun Y, Watt JA, Wang S, Lei S, Birnbaumer L, et al. Neurotoxin-induced ER stress in mouse dopaminergic neurons involves downregulation of TRPC1 and inhibition of AKT/mTOR signaling. J Clin Invest. 2012;122(4): 1354–67. [PubMed: 22446186]

[74]. Bollimuntha S, Singh BB, Shavali S, Sharma SK, Ebadi M. TRPC1-mediated inhibition of 1-methyl-4-phenylpyridinium ion neurotoxicity in human SH-SY5Y neuroblastoma cells. J Biol Chem. 2005;280(3):2132–40. [PubMed: 15542611]

[75]. Selvaraj S, Watt JA, Singh BB. TRPC1 inhibits apoptotic cell degeneration induced by dopaminergic neurotoxin MPTP/MPP(+). Cell Calcium. 2009;46(3):209–18. [PubMed: 19695701]

[76]. Sun Y, Zhang H, Selvaraj S, Sukumaran P, Lei S, Birnbaumer L, et al. Inhibition of L-Type Ca2+ channels by TRPC1-STIM1 complex is essential for the protection of dopaminergic neurons. J Neurosci. 2017;37(12):3364–77. [PubMed: 28258168]

[77]. McGurk JS, Shim S, Kim JY, Wen Z, Song H, Ming G-L. Postsynaptic TRPC1 function contributes to BDNF-induced synaptic potentiation at the developing neuromuscular junction. J Neurosci. 2011;31(41):14754–62. [PubMed: 21994391]

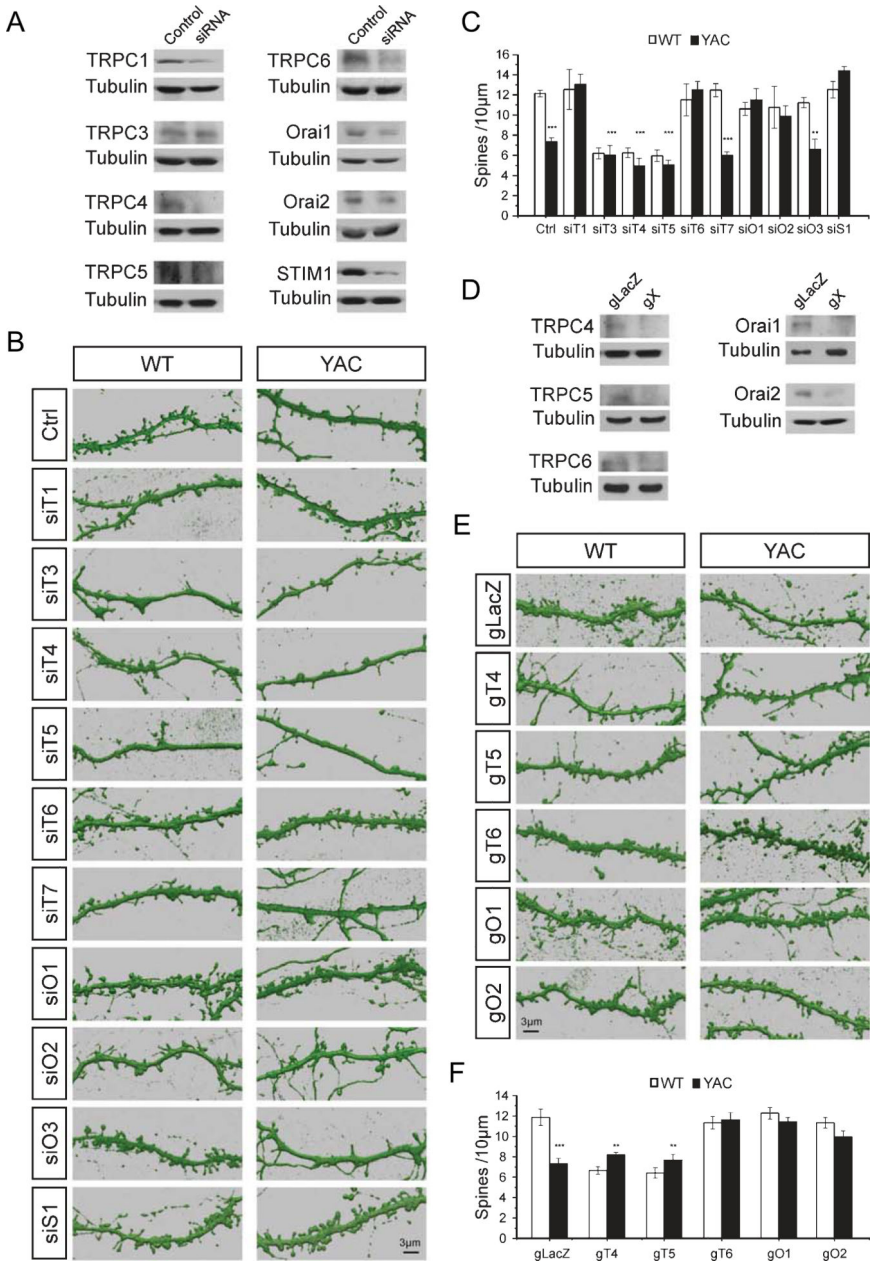

Fig. 1.

MSN spine density measurements in WT and YAC128 corticostriatal cultures. (A, D) Western blots of lysates from corticostriatal co-cultures after lenti-viral infection of neurons with siRNA (A) or Cas9/gRNA (D) targeting nSOC pathway components. The X in gX represents the indicated subunit. (B, E) 3D reconstructions from confocal images of DARPP32-immunostained MSN dendrites. Spines are shown for DIV 20 corticostriatal co-cultures prepared from WT and YAC128 pups. Co-cultures were infected with lentiviruses to express scrambled siRNA (Ctrl) or siRNA targeting TRPC1–7 (siT1-siT7), Orai1–3 (siO1-siO3), or STIM1 (siS1) (B). Co-cultures infected with lentiviruses to express Cas9 and control sgRNA (gLacZ), sgRNA targeting TRPC4–6 (gT4, gT5, gT6), or Orai1–2 (gO1, gO2) (E). (C, F) Quantification of spine density per 10μm of dendritic length in WT and

YAC128 cultures for RNAi knockdown experiments (C) and CRISPR/Cas9 knockout experiments (F). The results are shown as mean±S.E. (n=5–10). *p<0.05, **p<0.01, ***p<0.001 when compared to spine density in WT control cultures.

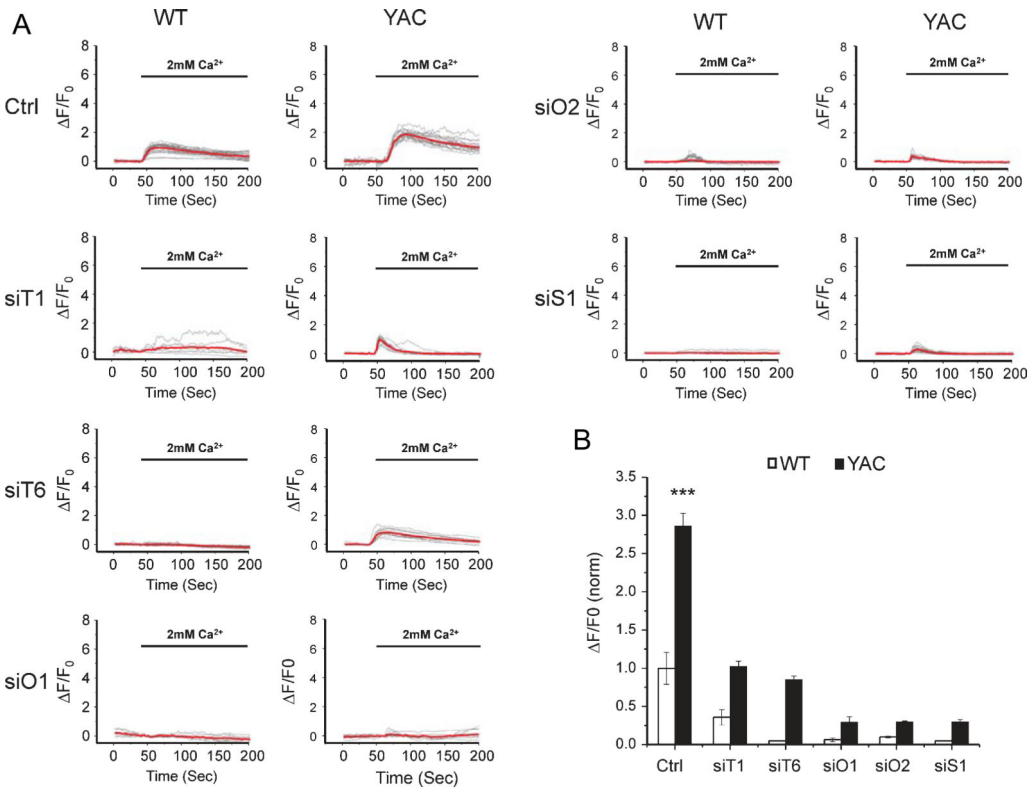

Fig. 2.

nSOC measurements in WT and YAC128 corticostriatal cultures. (A) GCaMP5G fluorescence traces in WT and YAC128 MSN spines following Ca^{2+} "add-back" protocol. The data are shown as change in relative GCaMP5G fluorescence over time. The time of "Ca^{2+} add-back" is shown above the fluorescence traces. Activity of SERCA pump in these experiments is blocked by 1μM thapsigargin (Tg). Individual cell traces are shown by thin grey lines, and average traces are shown by thick red lines. The traces are shown for cultures treated with control siRNA (Ctrl) and for the cultures treated with siRNA targeting TRPC1 (siT1), TRPC6 (siT6), Orai1 (siO1), Orai2 (siO2) or STIM1 (siS1). (B) Quantification of MSN spine nSOC in WT and YAC128 co-cultures expressing scrambled siRNA or siRNA targeting candidate nSOC channels or STIM1. The average peak of spine SOC was normalized to WT control cultures and shown as mean±SE (WT, n=15; YAC128, n=31; WT +siT1, n=13; YAC128+siT1, n=12; WT+siT6, n=20; YAC128+siT6, n=17; WT+siO1, n=9; YAC128+siO1, n=17; WT+siO2, n=19; YAC128+siO2, n=25; WT+siS1, n=15; YAC128+siS1, n=25). *** p<0.001 when compared to the nSOC amplitude in WT control cultures.

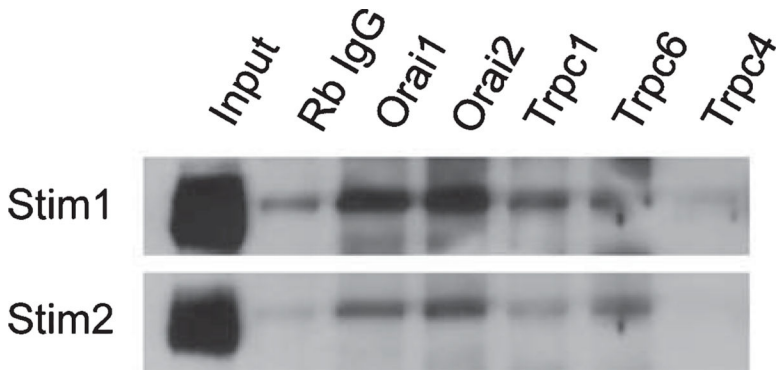

Fig. 3.

Association of candidate nSOC channels with STIM1 or STIM2 in synaptosomal lysates from WT striatum. Striatal synaptosomal lysates were prepared, solubilized and used in immunoprecipitation experiments with antibodies against Orai1, Orai2, TRPC1, TRPC6, and TRPC4. RabbitIgGwasusedasanegative control for the antibodies. Beads were washed, suspended in SDS loading buffer, boiled and analyzed by western blotting for STIM1 or STIM2.

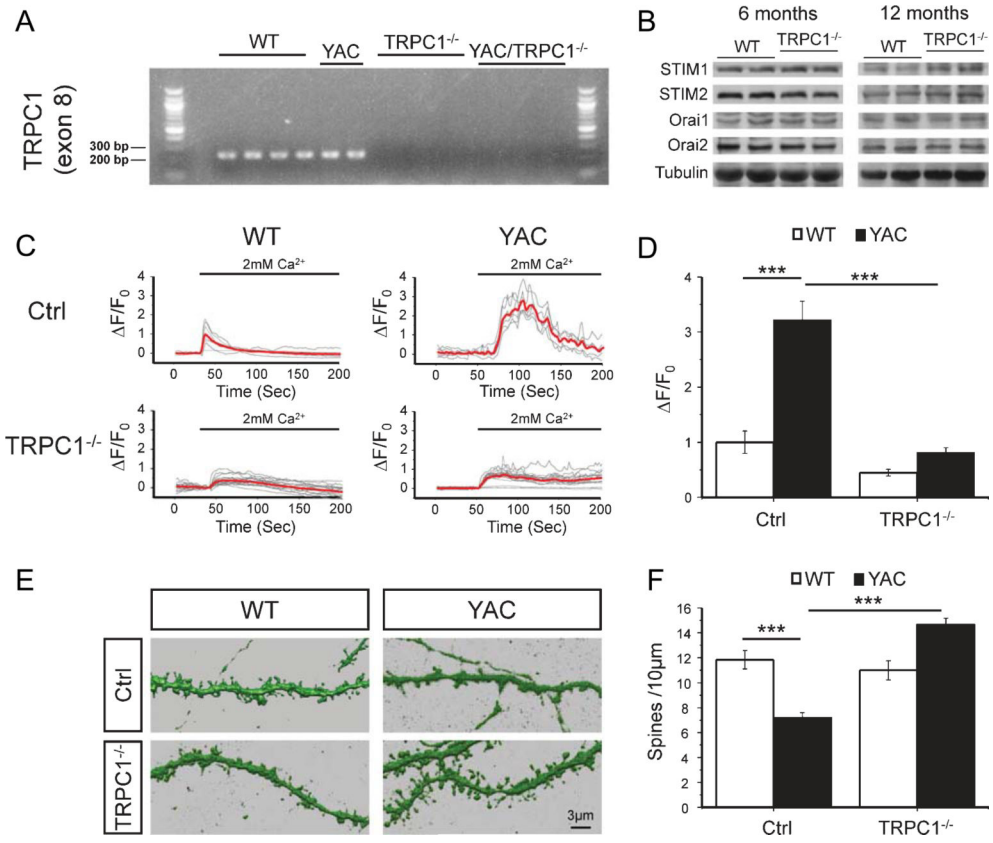

Fig. 4.

Knockout of TRPC1 prevents YAC128 MSN spine loss and reduces MSN spine nSOC. (A) RT-PCR was used to detect exon 8 of TRPC1 from WT, YAC128$^{+/-}$, TRPC1$^{-/-}$ and YAC128$^{+/-}$TRPC1$^{-/-}$ mice. (B) Striatal lysates from 6 months and 12 months old WT and TRPC1$^{-/-}$ mice were analyzed by western blotting for STIM1, STIM2, Orai1 and Orai2. (C) GCaMP5G was used to image spine Ca^2+ signals in response to calcium add back in co-cultures from WT, YAC128$^{+/-}$, TRPC1$^{-/-}$ and YAC128$^{+/-}$TRPC1$^{-/-}$ pups. The data are shown as change in relative GCaMP5G fluorescence over time. The time of "Ca^2+ add-back" is shown above the fluorescence traces. Activity of SERCA pump in these experiments is blocked by 1μM thapsigargin (Tg). Individual cell traces are shown by thin grey lines, and average traces are shown by thick red lines. (D) Quantification of spine nSOC. The average peak of spine SOC was normalized to peak nSOC in WT control cultures and shown as mean ± SE (WT, n=8; YAC128, n=6; TRPC1$^{-/-}$, n=17; and YAC128$^{+/-}$TRPC1$^{-/-}$, n=21). (E) Reconstructions from confocal images of DARPP32-immunostained MSN dendrites and spines are shown for DIV 20 corticostriatal co-cultures prepared from WT, YAC128$^{+/-}$, TRPC1$^{-/-}$ and YAC128$^{+/-}$TRPC1$^{-/-}$ pups. (F) Quantification of spine density. An average spine density in corticostriatal co-cultures is shown as mean ± SE (WT, n=10; YAC128, n=10; TRPC1$^{-/-}$, n=10; and YAC128$^{+/-}$TRPC1$^{-/-}$, n=10). ***p<0.001 for pairwise comparisons as shown.

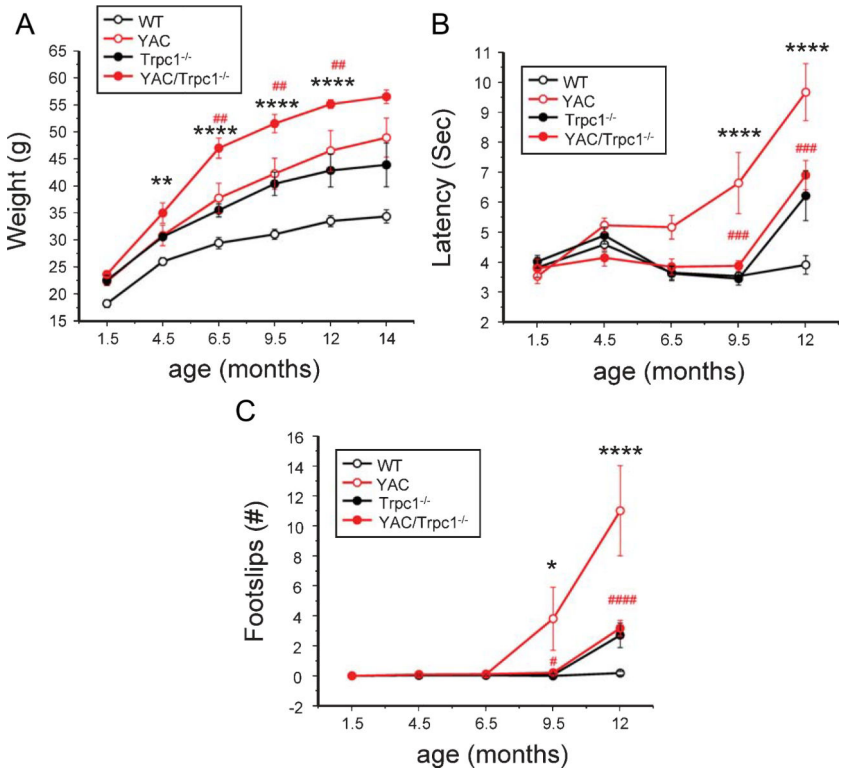

Fig. 5.

Knockout of TRPC1 improves motor performance of YAC128 mice in the beam walk assay. (A) Average body weight of WT, YAC128$^{+/-}$, TRPC1$^{-/-}$ and YAC128$^{+/-}$TRPC1$^{-/-}$ mice at different ages. (B) Beam crossing latencies and (C) number of foot slips for WT, YAC128$^{+/-}$, TRPC1$^{-/-}$ and YAC128$^{+/-}$TRPC1$^{-/-}$ mice at ages 1.5–12 months for the 17 mm beam are shown as mean ± SE (WT, n=14 female mice; YAC128, n=14 female mice; TRPC1$^{-/-}$, n=11 female mice; and YAC128$^{+/-}$TRPC1$^{-/-}$, n=11 female mice). *p<0.05, **p<0.01, ***p<0.001, ****p<0.0001 when the YAC128 group is compared to the WT group. $^{\#}p$<0.05, $^{\#\#}p$<0.01, $^{\#\#\#}p$<0.001, $^{\#\#\#\#}p$<0.0001 when the YAC128 group is compared to YAC128$^{+/-}$TRPC1$^{-/-}$ group.

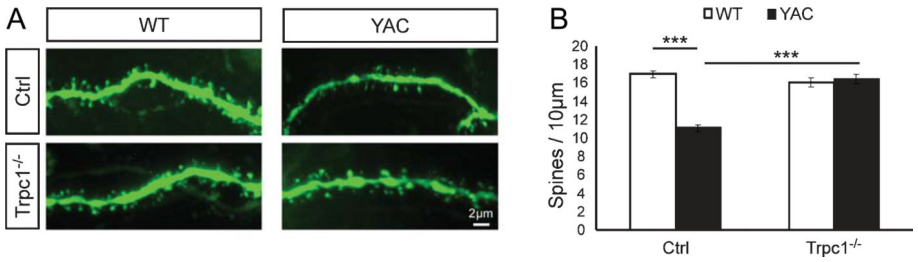

Fig. 6.

Knockout of TRPC1 prevents YAC128 MSN spine loss *in vivo*. (A) 14 months old WT, YAC128$^{+/-}$, TRPC1$^{-/-}$ and YAC128$^{+/-}$TRPC1$^{-/-}$ mice were perfused with fixative and MSNs in brain slices were microinjected with Lucifer yellow and visualized with2-photon microscopy.(B) Quantification of spine density in WT,YAC128$^{+/-}$,TRPC1$^{-/-}$ and YAC128$^{+/-}$TRPC1$^{-/-}$ mice.The average MSN spine density in striatal slices is shown as mean ± SE (WT, n=65; YAC128, n=101; TRPC1$^{-/-}$, n=47; and YAC128$^{+/-}$TRPC1$^{-/-}$, n=48). The data were pooled together from 8–13 mice for each group. ***p<0.001 for pairwise comparisons as shown.